IVYSPRING INTERNATIONAL PUBLISHER

Theranostics

2017; 7(13): 3387-3397. doi: 10.7150/thno.19748

Research Paper

Bone-Inspired Spatially Specific Piezoelectricity Induces Bone Regeneration

Peng Yu[1, 2], Chengyun Ning[1, 2]✉, Yu Zhang[3], Guoxin Tan[4], Zefeng Lin[3], Shaoxiang Liu[3], Xiaolan Wang[3], Haoqi Yang[3], Kang Li[3], Xin Yi[1, 2], Ye Zhu[5], Chuanbin Mao[5, 6]✉

1. School of Materials Science and Engineering, Biomedical Engineering Key Laboratory of Guangdong Province, South China University of Technology, Guangzhou, 510641, China;
2. Key Laboratory of Biomedical Sciences and Engineering, South China University of Technology, Guangzhou 510006, China;
3. General Hospital of Guangzhou Military Command of PLA, Guangzhou, 510010, China;
4. Institute of Chemical Engineering and Light Industry, Guangdong University of Technology, Guangzhou, 510006, China;
5. Department of Chemistry and Biochemistry, Stephenson Life Sciences Research Center, University of Oklahoma, Norman OK 73019, USA;
6. School of Materials Science and Engineering, Zhejiang University, Hangzhou, Zhejiang 310027, China.

✉ Corresponding authors: Prof. C. Y. Ning, School of Materials Science and Engineering, South China University of Technology (China), Wushan RD., TianHe District, Guangzhou, 510640, China E-mail: imcyning@scut.edu.cn Phone: +86 020-22236882 Prof. C. B. Mao, Department of Chemistry & Biochemistry, Stephenson Life Sciences Research Center, University of Oklahoma (USA) E-mail: cbmao@ou.edu

Received: 2017.02.20; Accepted: 2017.05.18; Published: 2017.08.11

Abstract

The extracellular matrix of bone can be pictured as a material made of parallel interspersed domains of fibrous piezoelectric collagenous materials and non-piezoelectric non-collagenous materials. To mimic this feature for enhanced bone regeneration, a material made of two parallel interspersed domains, with higher and lower piezoelectricity, respectively, is constructed to form microscale piezoelectric zones (MPZs). The MPZs are produced using a versatile and effective laser-irradiation technique in which $K_{0.5}Na_{0.5}NbO_3$ (KNN) ceramics are selectively irradiated to achieve microzone phase transitions. The phase structure of the laser-irradiated microzones is changed from a mixture of orthorhombic and tetragonal phases (with higher piezoelectricity) to a tetragonal dominant phase (with lower piezoelectricity). The microzoned piezoelectricity distribution results in spatially specific surface charge distribution, enabling the MPZs to bear bone-like microscale electric cues. Hence, the MPZs induce osteogenic differentiation of stem cells *in vitro* and bone regeneration *in vivo* even without being seeded with stem cells. The concept of mimicking the spatially specific piezoelectricity in bone will facilitate future research on the rational design of tissue regenerative materials.

Key words: electrical cues; piezoelectricity; bone; tissue regeneration; stem cells.

Introduction

Reconstructuring the microenvironment in which the stem cells live is one promising approach to the design of regenerative biomaterials [1]. The stiffness, nanotopography and chemistry of the biomaterials are frequently designed to mimic the signal information present in the native tissue microenvironment to modulate stem cell differentiation and tissue regeneration [2-6]. Engler et al. discovered that the mesenchymal stem cells (MSCs) lineage specification is sensitive to the elasticity of the extracellular envirionment [7], which has inspired many studies on the use of materials stiffness to modulate stem cell behaviors [8, 9]. Moreover, many researchers have shown that the micro/nano-topographies could provide mechanoregulation to drive the differentiation of MSCs [10-12]. All above studies on the effects of the physical cues on the cell/materials interactions will advance the therapeutic uses of stem cells. However, the physiological electro-microenvironment of a target tissue is rarely considered during the design of tissue regenerative biomaterials. In fact,

piezoelectricity is naturally present in the human body though it has not been fully explored for regenerating tissue.

For instance, the piezoelectricity of living bone is fundamental for the growth of bone as well as the repair of bone fractures [13-16]. Previous studies have demonstrated that the origin of the piezoelectric phenomenon in bones could be attributed to the aligned collagen molecules, which are the basic organic component of natural bone [17]. Collagen molecules are parallel-aligned into fibrils and become mineralized to form the extracellular matrix of bone [18, 19]. Namely, due to the piezoelectricity of collagen fibrils, the extracellular matrix of bone can be pictured as parallel interspersed domains of fibrous piezoelectric collagenous materials and non-piezoelectric non-collagenous materials, resulting in the spatially specific positive charges localized on the collagenous domains (**Figure 1a**) [20]. In addition, it is proposed that an external electrical cue, though not arising from piezoelectricity, can modulate stem cell behaviors [21-24]. Hence, we believe that mimicking interspersed piezoelectric microzones in bone is an alternative strategy for inducing bone formation on the orthopedic implants (**Figure 1b**). Specifically, we propose to form two parallel microzones (with higher and lower piezoelectricity) on an implant to mimic the distribution of collagenous (piezoelectric) and non-collagenous (non-piezoelectric) domains. Then we evaluate the capability of the resultant implants, termed microscale piezoelectric zones (MPZs), in inducing osteogenic differentiation *in vitro* and bone formation *in vivo* (**Figure 1b**).

To prove our hypothesis, for the first time, we employed piezoelectric $K_{0.5}Na_{0.5}NbO_3$ (KNN) ceramics to produce MPZs. The displacement of atoms in the KNN crystalline lattice could induce phase change of KNN [25, 26]. To construct MPZs, the surface of KNN originally made of a mixture of orthorhombic and tetragonal phases with higher piezoelectricity is selectively heated by laser to induce the phase change, where orthorhombic phase is converted into tetragonal phase. Namely, the laser-irradiated KNN area (termed LK) is of lower piezoelectricity than the pristine non-irradiated KNN area (termed PK). Surprisingly, the bone-mimetic MPZs induced osteogenic differentiation and bone regeneration more efficiently than the original KNN and other control non-piezoelectric substrates such as hydroxyapatite (HA).

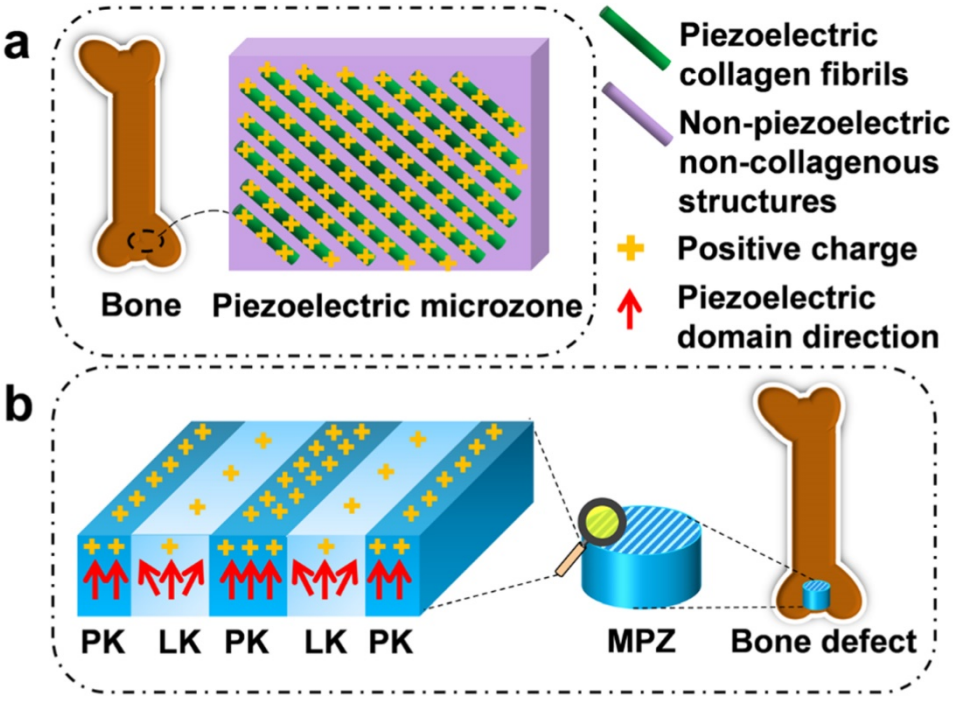

Figure 1. Construction of microscale piezoelectric zones (MPZs) to mimic piezoelectric microzones in natural bone for bone defects repair. a) The parallel piezoelectric collagen fibers (separated by non-piezoelectric zones) in living bone can generate parallel collagenous domains of a positive charge (due to the unique interspersed distribution of piezoelectric and non-piezoelectric domains), representing an *in vivo* physiological electro-microenvironment. b) To mimic such electro-microenvironment resulting from piezoelectric collagen fibers, MPZs were fabricated by set-selective laser irradiation and poling on the KNN surface (Middle) and then implanted into bone defect model to evaluate the bone regeneration on the MPZs. PK stands for non-irradiated pristine KNN zone, which preserves the original structure of a higher piezoelectricity and mimics the piezoelectric collagenous fibers in bone (a). LK stands for laser-irradiated KNN zone, which presents a lower piezoelectricity and mimics the non-piezoelectric domains in natural bone (a). The red arrows show the direction of piezoelectric domains of the MPZs. More positive charges were generated on the PK zone than on the LK zone (due to the interspersed distribution of domains of higher and lower piezoelectricity) after poling to mimic *in vivo* physiological electro-microenvironment.

Materials and methods

Construction of MPZs on KNN ceramics

The potassium carbonate (99.0%, Aladdin, China), sodium carbonate (99.5%, Aladdin, China) and niobium oxide (99.99%, Aladdin, China) were mixed at a molar ratio of 1:1:2 to prepare $K_{0.5}Na_{0.5}NbO_3$ (KNN) samples. The raw materials were ball-milled in ethanol at 250 rpm for 12 h and then dried at 75 °C for 24 h. The dried powders were calcinated at 750 °C for 2 h, and then 8 wt % poly(vinyl alcohol) (PVA, Aladdin, China) was added to the calcinated powders for granulation. The granular powders were uniaxially compressed into disk-shaped samples under 200 MPa for 30 min through cold-isostatic pressing. These pellet samples were sintered in an electric muffle furnace at 1080℃ for 2 h. To acquire bone-like, relatively lower piezoelectric properties, the samples were subsequently polarized under an applied electric field of ~5 kV/cm for 20 min. HA nanopowder (Aladdin, biomedical grade) was also uniaxially compressed into disk-shaped samples under 200 MPa for 30 min through cold-isostatic pressing. The compressed samples were sintered at 1200 °C for 4 h to acquire the control group samples (termed HA group). KNN and HA samples were then subjected to gradient grinding with abrasive paper of different grades (1000#, 2000#, 3000# and 5000#). The focused laser beam, exerted by an IPG solid-state laser (λ=1064 nm, Handslaser, China), was used to induce microzone phase transitions to construct the MPZs on the KNN. The laser parameters of power and laser scanning speed were set as 2.8 W and 100 mm/s, respectively. The intervals of the MPZs could be adjusted by using the CAD software (HL software, Handslaser, China) to manipulate laser canning pathways.

MPZs characterization

The morphology and element distribution of the MPZs were characterized using a scanning electron microscope (SEM) and an energy dispersive spectrometer. Piezoelectric force microscopy (PFM, MFP-3D, Asylum Research, USA) was used for piezoelectricity examination. For the PFM observations, the sintered KNN samples were ground to approximately 200 μm and then polished with polycrystalline diamond paste with abrasive particles of up to 3 μm. The PFM signal was acquired under an AC voltage of 1-5 V and a frequency of 50 kHz. Scanning Kelvin probe microscopy (SKPM) was employed to analyze the surface potential difference at the micro-boarder of MPZs. Surface roughness of the MPZs and controls was analyzed using the atomic force microscopy (AFM). Each analysis was performed in a 20 μm × 20 μm area. The piezoelectric coefficient d_{33} of the groups was determined using a quasi-static piezoelectric constant testing meter (YE2730A, Yutian Technology Co. Ltd., China).

In vitro cell culturing and seeding

For sterilization, both sides of samples were exposed under an ultraviolet ray for 30 min after immersed in 70% ethanol for 60 min. Mouse bone marrow-derived mesenchymal stem cells (BMSCs) were purchased from ATCC (CRL-12424, ATCC, USA), and BMSCs before passage 5 were used for the *in vitro* assay. The BMSCs suspended in normal growth media (10% FBS+DMEM, Gibco) were seeded on the samples surface for the morphological observations and the osteogenesis experiments. The cells were cultured in a humidified atmosphere with 5% CO_2.

Actin staining and BMSCs proliferation

Actin staining was conducted to examine the BMSCs morphology on the MPZs and control surfaces. BMSCs cultured for 3 days were used for actin staining. To stain the cells, the cells on the samples surface were fixed with 4% paraformaldehyde for 10 min, and then permeabilized in 0.1% Triton X-100 solution for 5 min. After washed with PBS containing 0.1% Triton X-100, the samples were stained with an Actin-Tracker Green (Beyotime, Beijing, China) solution. The cytoskeleton of the stem cells was observed by a confocal laser scanning microscope (TSC SPE, Carl Zeiss Group, Germany). The aspect ratio of the BMSCs on MPZs and controls was determined by analyzing their Actin-Tracker Green fluorescent images using image J software (National Institutes of Health, USA). Proliferation of BMSCs was determined using Quant-iT dsDNA Assay (PicoGreen, Invitrogen, USA). The BMSCs were cultured for 1, 3 and 5 days, and washed with sterilized PBS and stored at -80 ℃. The samples were exposed to proteinase K to release dsDNA. 10 μL dsDNA supernatant was mixed with 10 μL PicoGreen reagent in dark room for 5 min. The mixture was then measured using a spectral scanning multimode reader (Varioskan Flash, Thermo-Fisher Scientific, UK).

In vitro osteogenesis assay

After cultured for 7 days, the BMSCs were lysed to measure the alkaline phosphatase (ALP) activity, by quantifying the converted yellow p-nitrophenol (pNP) at 405 nm. The ALP activity divided by the cell protein concentration was obtained to quantify the osteogenic properties of the BMSCs cultured on MPZs and controls. For ALP staining assay, the BMSCs

cultured for 7 days were stained using BCIP/NBT Alkaline Phosphatase Color Development Kit (Beyotime, Beijing, China). The photographs of the stained samples were taken using digital camera (D7110, Nikon, Japan).

Immunofluorescent staining of Runx2, Col I and OPN expression was used for examining the osteogenic markers. BMSCs was seeded on the MPZs and controls for 7 days (for Runx2 assay) and 14 days (for OPN and Col I assay). The samples were rinsed with PBS for three times and fixed with 4% paraformaldehyde for 15 min. After washed for three times, the fixed cells were penetrated with 0.1% Triton X-100 for 15 min. The 1% PBS solution of bovine serum albumin was used to block the samples. After the block solution was removed, the anti-Runx2 antibody (ab23981, Abcam), anti-Collagen I antibody (ab34710, Abcam) and anti-OPN antibody (ab91655, Abcam) diluted at a ratio of 1:100 were added to the samples surface, respectively, and the mixtures were incubated at 37 °C for 1 h in dark. Then the samples were cultivated with goat anti-rabbit IgG antibody (bs-0295G-HRP, Bioss, China) for 30 min. The immunostained samples were observed by a confocal laser scanning microscope (SP8, Leica, Germany). Further quantitative analysis of the fluorescent images of the stained proteins was done using the image J software. The quantified fluorescence intensity of the osteogenic proteins was normalized to the fluorescence intensity of the DAPI staining the cell nuclei. To examine the piezoelectric stability of the samples in the biological systems, the samples were immersed in DMEM solution for 30 days. Then the samples were rinsed with PBS and dried before the measurement of the piezoelectric coefficient d_{33}.

Evaluation of the *in vivo* osteogenic performance of the MPZs

A rabbit formal condyle bone defect model, which is a load-bearing defect model, was created to evaluate the bone regeneration performance of MPZs *in vivo*. The research was approved by the Animal Care and Use Committee of General Hospital of Guangzhou Military Command of PLA. Twelve male New Zealand rabbits (3 month old, ~2.5 kg) were randomized into 3 groups and anesthetized with pentobarbital sodium. To generate defect models, defects (5 mm long and 3 mm wide) parallel to the long axis of the femur were created at the knee joint capsule of both femurs of each rabbit. Two samples were implanted into each animal, with one sample in one of the two legs. The polarized MPZs specimens and their controls were implanted into the defect site. For KNN and the MPZs samples, they were placed into the defect sites in such a way that the positively polarized side faced the deep side of bone marrow cavity. The animals were sacrificed to evaluate the bone formation using micro-computed tomography (micro-CT) (Latheta, Aloka co., LTD, Tokyo, Japan) after implantation for four weeks. The three-dimensional structure of the newly built bone on the femoral peri-implant region was reconstructed using Mimics software (version 14.11, Materialise, Belgium). After Micro-CT scanning, the samples were dehydrated in gradiently concentrated ethanol. Then the dehydrated samples were embeded in light-curing epoxy resin (Technovit 7200VLC, HereausKulzer, Wehrheim, Germany) through light polymerization. The embeded samples were bonded to the plastics slide and sectioned along the parallel direction of the long axis of the implants to get a slice with a thickness about 100 μm using a saw microtome (EXAKT-300CP, German). Then the bonded slices of samples were grounded to about 20 μm thick using a grinding machine (EXAKT-400CS, German). Then the sections of specimens were used for H&E staining and backscattered SEM observation [27].

Statistical analysis

All of the data are presented as the mean ± standard deviation. Significant differences were determined using a one-way analysis of variance (ANOVA) in SPSS 17 (IBM, Armonk, New York, USA) software ($n = 4$, $^{**}p < 0.01$, $^{*}p < 0.05$).

Results and Discussion

Construction and characterization of the MPZs

KNN ceramics prepared by conventional pressing and sintering were used in this research. A computer-controlled focused laser beam was used to perform site-specific irradiation of the KNN to convert selected zones to low piezoelectricity phases, resulting in periodically organized LK and PK zones on the KNN surface. When a laser beam at the proper power was irradiated upon the KNN surface, the absorbed laser energy was rapidly converted to local heat, which raised the temperature and induced compositional and phase transitions in a confined microscale area [28]. Finally, the periodic distribution of microscale piezoelectric PK and LK zones could be adjusted by simply designing the laser scanning distance using a computer program **(Figure 2a).** Energy-dispersive X-ray spectroscopy (EDS) and X-ray diffraction (XRD) analyses were conducted to examine the element and phase compositions to explore the source of different piezoelectricity on the MPZs (Figure 2b-d). EDS mapping (Figure 2b and c) confirmed that there is a significant decrease in Na

and K elemental compositions in the LK zones compared with that of the PK zones. This decrease was generated through element evaporation induced by the temperature increase during laser irradiation as expressed in equation (1).

$$2\mathrm{M}_M^* + \frac{1}{2}O_2 \xrightarrow{\Delta} M_2O \uparrow + 2V_M' + 2h^* \quad (1)$$

where M represents the alkali elements (Na and K) and V and h represent vacancy and electrons, respectively. It should be noted that the volatility of the alkali elements reduces the piezoelectricity of the LK zone [29]. The piezoelectric performance of KNN-based ceramics is known to be dictated by the perovskite phase structure. The phase composition of non-irradiated KNN (representing the PK zone) and completely irradiated KNN (representing the LK zone) were examined through XRD spectra as shown in Figure 2d. To determine the phase composition of the PK and LK zones, we assessed the relative intensities of (002) and (200) peaks, which are magnified in the inset of Figure 2d. For the orthorhombic phase, this ratio (I_{002}/I_{200}) is approximately 2:1, whereas for the tetragonal phase, the ratio is 1:2 [30, 31]. For pristine KNN, the (200) and (002) peaks were of similar magnitude, which indicates the co-existing of orthorhombic and tetragonal phases. However, for the laser-irradiated KNN, the (002) peak was much weaker than the (200) peak, indicating that the tetragonal phase was more pronounced and demonstrating that the high temperature caused by laser irradiation changed the phase composition. It is known that when the amount of the tetragonal phase is increased in the binary phase mixture, the piezoelectricity will be reduced [31]. These results indicate that the piezoelectricity of the PK zone would be higher than that of the LK zone.

Electrical performance of MPZs

The piezoelectricity of the PK and LK zones were compared. PFM was used to measure the piezoelectric response of the non-irradiated KNN and completely irradiated KNN samples. For the non-irradiated KNN and completely irradiated KNN samples, the phase (**Figure S1a, b**) and amplitude mappings (Figure 2e, f) of the PFM images were consistent. The amplitude piezoresponse of the non-irradiated KNN and completely irradiated KNN samples were averaged to ~220.2 pm and 6.2 pm under 1 V AC and 5 V AC, respectively. The results suggested that the non-irradiated KNN samples produced excellent piezoelectricity. They also confirmed that the non-irradiated KNN sample produced a greater piezoelectric response than the completely irradiated KNN sample [32, 33], implying that PK zone would have higher piezoelectricity than the LK zone. Finally, the surface potentials of the polarized PK and LK zones were measured on the MPZs to confirm the spatially specific electrical cue caused by differences in piezoelectricity. We examined the surface potential of the borders between the PK and LK zones by SKPM

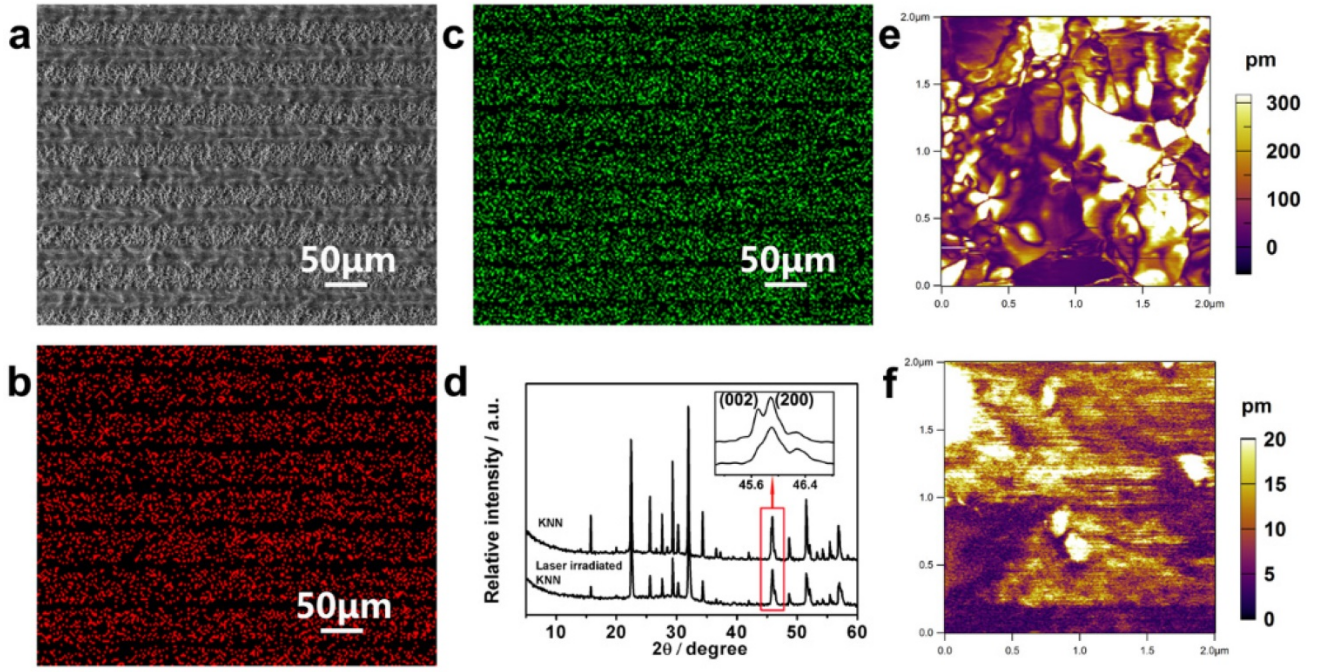

Figure 2. Construction and characteristics of the MPZs. a) SEM image of constructed MPZs with 50 μm domain intervals on the KNN surface. b, c) Elemental mapping (b, Na; and c, K) of the MPZs surface. d) XRD patterns of pristine KNN and laser-irradiated KNN. The inset is the magnified image of the XRD patterns at approximately 45°. The XRD results indicate that the pristine KNN is mainly composed of orthorhombic and tetragonal phases, whereas laser-irradiated KNN is mainly composed of a tetragonal phase. e and f) Amplitude mapping of the vertical PFM of pristine KNN (~220 pm) and laser-irradiated KNN (~6 pm). The results indicate that periodic microscale zones with different piezoelectricity were constructed.

to determine the surface potential difference between the PK and LK zones. The SKPM analysis indicated that the surface potential of the LK zone was negatively shifted by ~59 mV compared with that of the PK zone (Figure S1c), which confirmed the surface potential difference between the PK and LK zones after poling. The MPZs with specific piezoelectricity was expected to provide electrical cue to simulate the *in vivo* bone electro-microenvironment.

The evaluation of the *in vitro* BMSCs behaviors on MPZs and controls

To determine whether biomimetic MPZs can induce and promote osteogenic differentiation, two control groups, KNN (unmodified but polarized) and HA discs were prepared. HA is a component of bone and has been widely used as a bone repairing material [34]. In this research, the HA samples were prepared by the cold-isostatic pressing and sintering of the biomedical grade HA nanopowder (**Figure S2**). The EDS (Figure S2a, inlet) and XRD (Figure S2b) spectra indicate that the sintered ceramics were indeed HA. AFM characterization indicates that the surface roughness of the KNN group, PK-zone of MPZ group and HA group was similar (Figure S3) whereas the surface roughness of the LK-zone of the MPZ group was lower than the KNN group due to laser irradiation. Prior to the cell culture experiments, all the KNN and MPZs group samples were polarized under an applied electric field (~**5** kV/cm). First, we examined the ability of BMSCs to proliferate on the MPZs using a Quant-iT dsDNA Assay (**Figure 3a**). On day 3, the HA group showed a higher cell proliferation rate than the MPZs and KNN group. The cell proliferation rate should have been influenced by the polarization of the BMSCs on the charged KNN and MPZs surfaces [35-37]. However, the cell proliferation rate of the MPZs surpassed that of KNN and HA controls on day 5, indicating that the MPZs proliferated well after 5 days of culture.

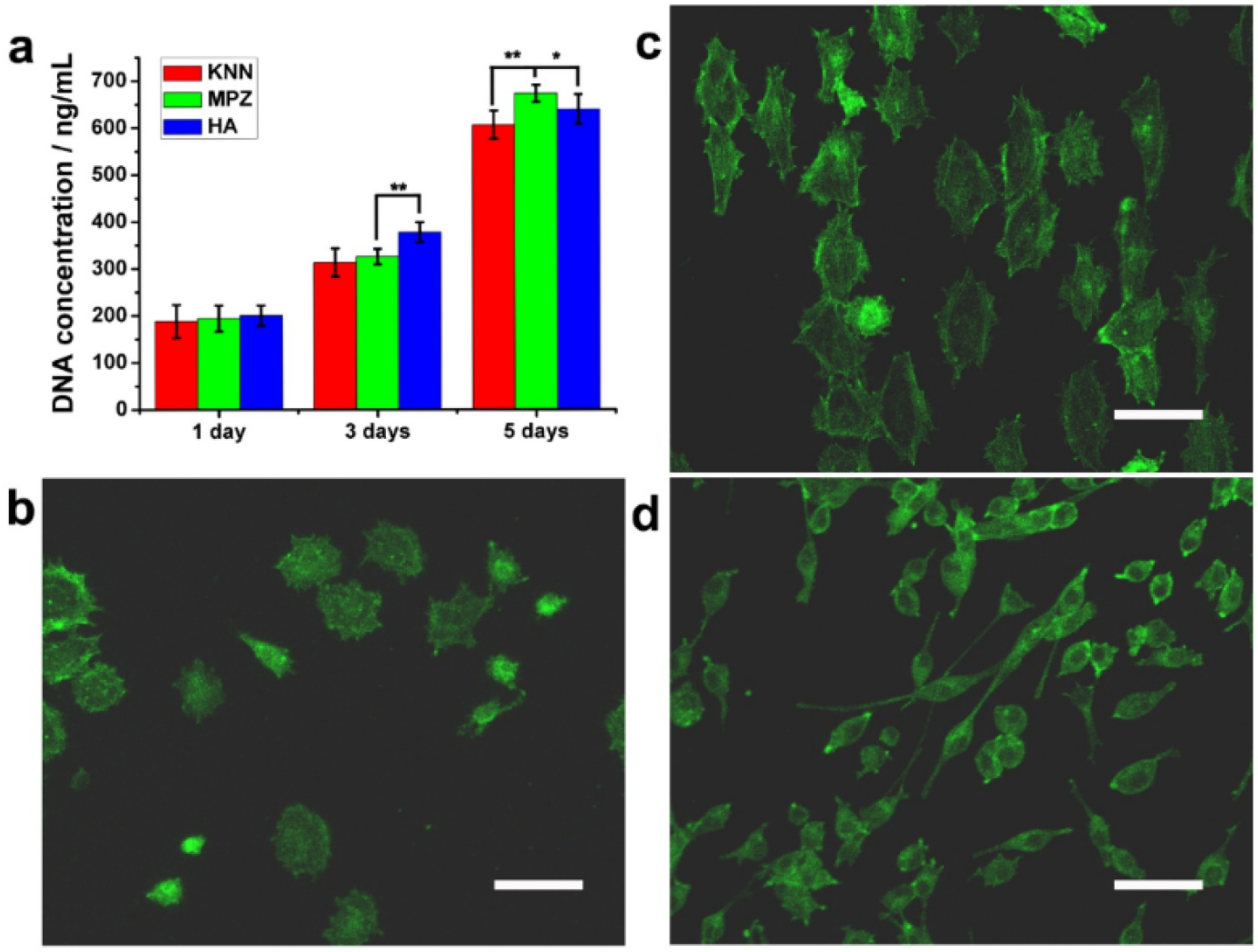

Figure 3. Morphology, proliferation and differentiation of BMSCs on the MPZs and control surfaces. a) Quant-iT dsDNA Assay of BMSCs on the samples. The assay was repeated twice and expressed as means ± s.d.. Significant differences were determined using a one-way analysis of variance (ANOVA) followed by LSD-t test. (**) and (*) indicates a statisctic difference at $p < 0.01$ and $p < 0.05$, n=6. b-d) Fluorescence images of the actin skeletons of BMSCs on the MPZs surface and control samples after cultured for 3 days: b) polarized KNN, c) MPZs, d) HA. Scale bar: 75 μm. These images show that BMSCs on the MPZs are elongated and aligned along the MPZs substrate. The BMSCs on HA show a reduced adhesion area. F-actin was stained by FITC-labeled phalloidin (green).

To further examine the cell morphology, immunofluorescent staining of the actin cytoskeleton with phalloidin was conducted on day 3. The BMSCs on the MPZ and KNN groups showed a relatively large spreading area compared with the cells on the HA surface, which indicated that the KNN and MPZ groups could promote cell attachment. Since we cultured the cells on the positively polarized side of the piezoelectric materials, this discovery is in accordance with previous studies where the positively charged surfaces were found to promote cell attachment and spreading [38, 39]. The electrostatic force between the positively charged samples (KNN or MPZs) and BMSCs (negatively charged in a physiological environment) would promote cell attachment and spreading. In addition, the BMSCs on the MPZs showed a larger aspect ratio than those on the KNN group and were aligned along the direction parallel to the border of the PK and LK zones (Figure 3b-d and S4). The modulation of the cell orientation and morphology was attributed to the spatially distributed electrical cue of MPZs. After the BMSCs were seeded on the MPZs, they could sense and respond to the electrical cue above the MPZs through the charged surface proteins and glycoproteins, inducing endogenous bioelectrical signals that modulated cell adhesion [23, 40]. The cell morphology, proper aspect ratio and cytoskeleton orientation would further influence BMSCs differentiation [41].

To examine the effect of MPZs on BMSCs differentiation, the activity of ALP, an early-stage osteogenic marker, was determined. ALP staining was conducted on the MPZs and control groups. The cells were cultured in growth media (i.e., non-osteogenic media) to exclude the influence of osteogenic inducers in the media. Both the colorimetric ALP enzymatic activity assay kit (**Figure 4a**) and ALP enzymatic staining (Figure 4b) results suggested that the MPZs significantly promoted the expression of ALP compared with the other groups. An almost three-fold promotion of ALP expression could be observed on the MPZs on day 7 compared with that on the KNN group, suggesting that MPZs could more efficiently simulate the *in vivo* bone electro-microenvironment to promote osteogenic differentiation of BMSCs. Meanwhile, the MPZs also significantly promote the expression of ALP compared to the un-polarized MPZ (U-MPZ, not charged on the surface), which means that it is the spatially distributed charges that makes MPZs promote osteogenic differentiation.

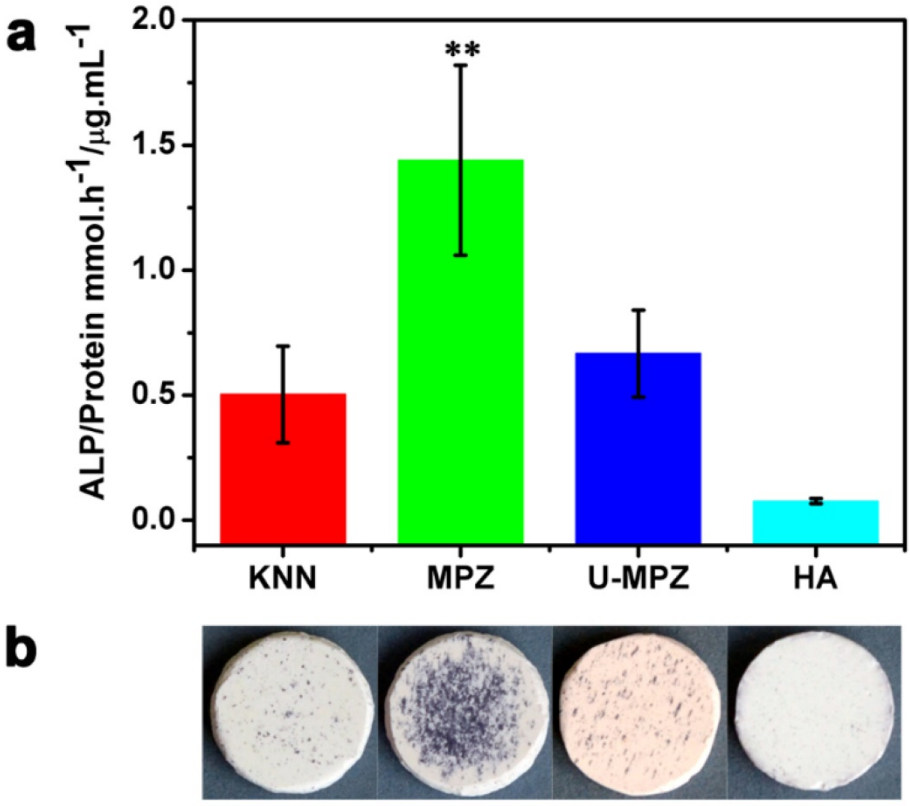

Figure 4. ALP enzymatic activity analysis. a) ALP enzymatic activity of the BMSCs cultured on samples in non-osteogenic growth media for 7 days; the results show that MPZs significantly upregulate ALP activity. The assay was repeated twice and expressed as means ± s.d.. Significant differences were determined using Kruskal-Wallis Test. (**) indicates a significant difference at $p < 0.01$ compared to HA condition, n=4. b) Osteogenic differentiation visualized by ALP enzymatic staining after 7 days of incubation in growth media; the results suggest that MPZs induce osteogenic differentiation even in non-osteogenic media. KNN: unmodified but polarized KNN; MPZ: modified and polarized KNN; U-MPZ: modified but un-polarized KNN; HA: non-polarized hydroxyapatite.

The osteogenic differentiation of BMSCs cultured on MPZs and controls was further evaluated by examining the expression of osteogenic markers. Runt related transcription factor 2 (Runx2), Collagen I (Col I) and osteopontin (OPN) are the main extracellular matrix (ECM) proteins secreted during the osteogenic process. The Runx2 could regulate osteogenic gene expression and is essential for osteogenic differentiation. Both OPN and Col I function in the formation of bone nodules to develop mineralized bone [42, 43]. After cultured with MPZs and controls for 7 days, the cells were immunostained for Runx2 (**Figure 5 and S5**). The cells cultured on the MPZs show enhanced expression of Runx2 compared to the KNN, U-MPZ and HA groups, which is indicated by the immunofluorescent intensity. Quantitative analysis of the stained proteins also suggested the superior enhanced expression of Runx2 by the BMSCs on the MPZs. Moreover, the cells were immunostained for the Col I and OPN (**Figure 5**) after cultured with MPZs and controls for 14 days. The cells cultured on the MPZs also show enhanced expression of Col I compared to the KNN, U-MPZ and HA. An obvious promotion in the expression of OPN by the MPZ group compared to other control substrates is also observed in Figure 5 and S5. The osteogenic markers analysis indicated that the MPZs induced the osteogenic differentiation of BMSCs. The fact that both KNN and U-MPZ are not as osteogenic as MPZs suggests that the surface charge as well as its spatial distribution, resulting from the unique bone-like microzoned distribution of PK and LK with higher and lower piezoelectricity respectively, are essential for MPZs to achieve effective osteogenesis. Although the surface roughness of the LK-zone of the MPZ group was significantly lower than that of the PK-zone (of the MPZ group) and the KNN group (Figure S3), the poor osteogenic performance of the U-MPZ control group compared to the MPZ group confirmed that the influence of surface roughness to the stem cell differentiation could be ignored compared to the microzoned distribution of piezoelectricity. To test the stability of the piezoelectricity of the MPZs, the MPZs were immersed in DMEM solution for 30 days. The results indicate that the immersed samples presented a piezoelectric coefficient d_{33} of 4.86±0.98 pC/N, which is close to the original piezoelectric coefficient d_{33} of 4.99±0.91 pC/N.

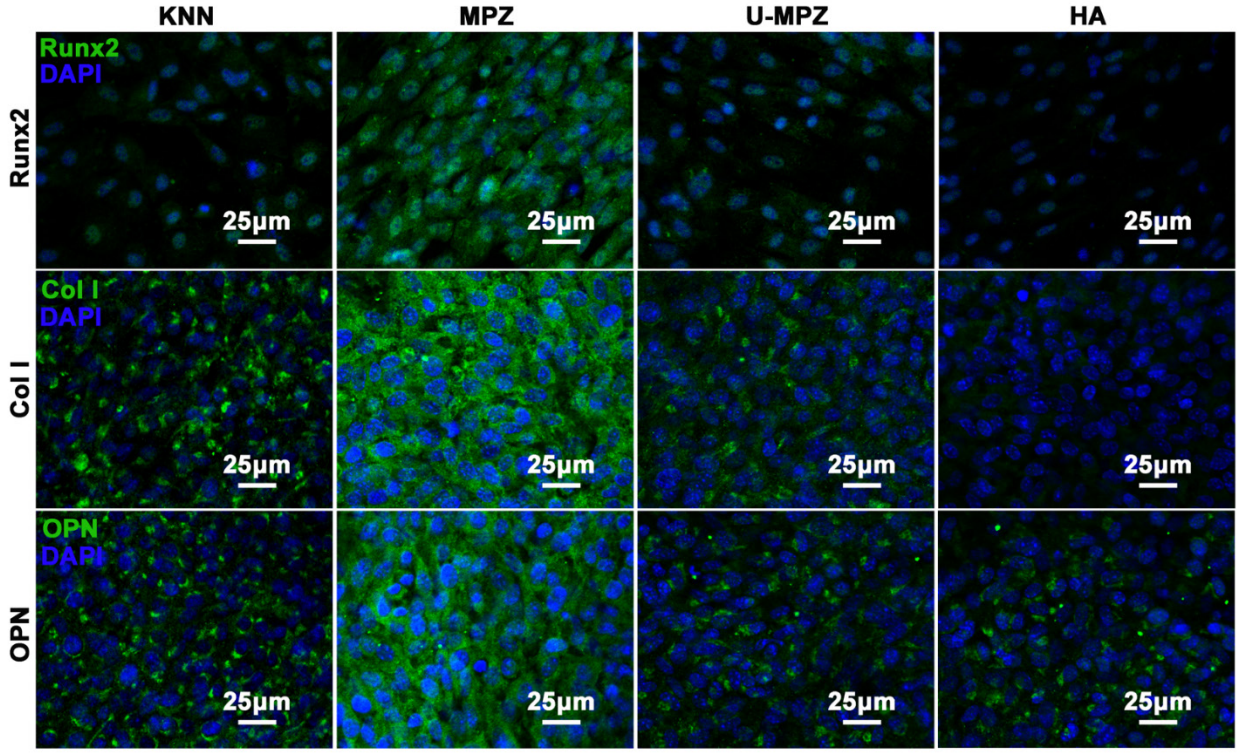

Figure 5. Immunocytochemistry of osteogenic protein, Runx2, Col Ⅰ and OPN, expressed by BMSCs cultured on different substrates in non-osteogenic growth media for 7 days (Runx2) and 14 days (Col Ⅰ and OPN). The results indicate that the MPZs promote the expression of Runx2, Col Ⅰ and OPN compared to the controls. The Runx2, Col Ⅰ and OPN were stained in green color with FITC. The nuclear stain is in dark blue with DAPI. KNN: unmodified but polarized KNN; MPZ: modified but polarized KNN; U-MPZ: modified but un-polarized KNN; HA: non-polarized hydroxyapatite.

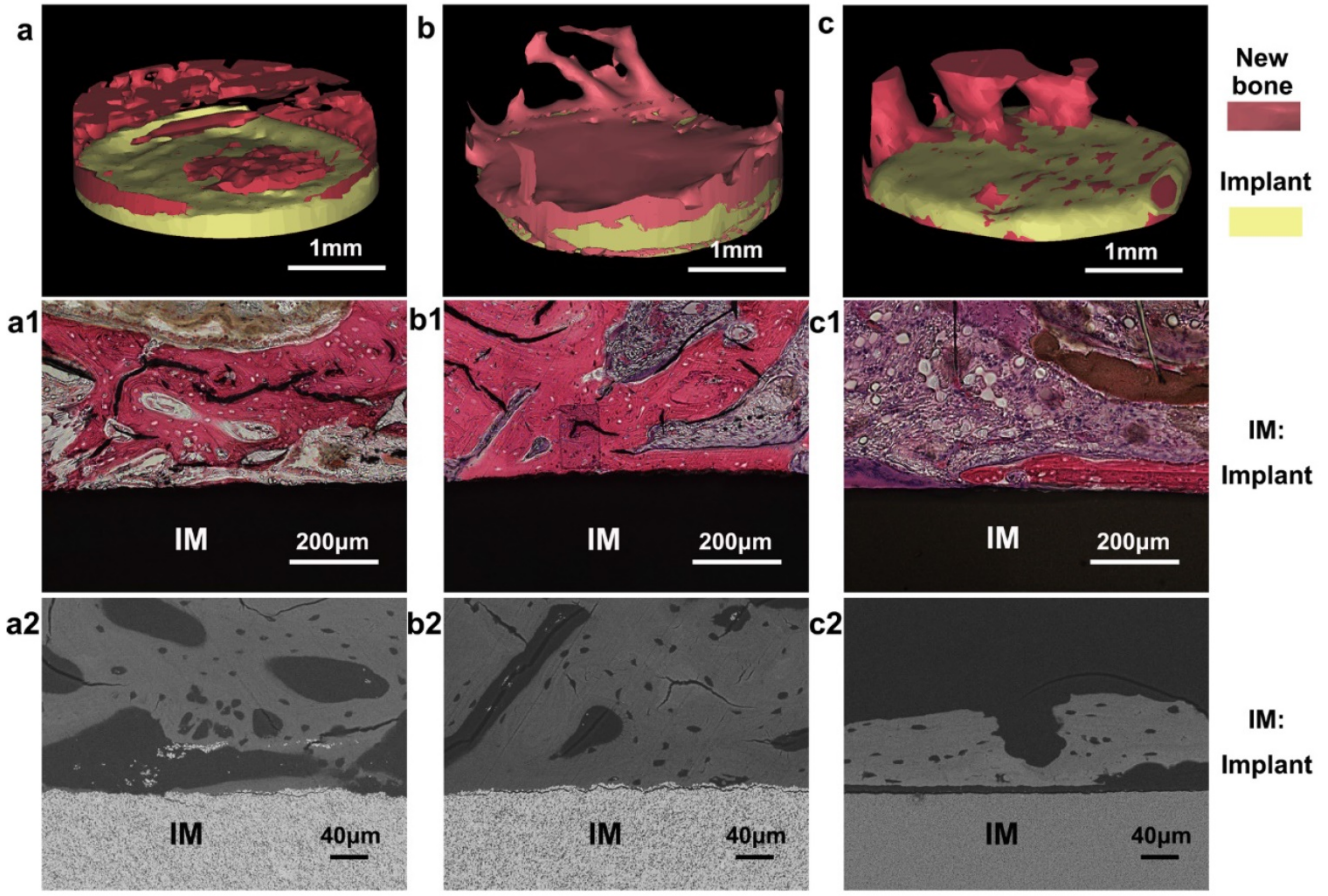

Figure 6. *In vivo* osteogenesis on cylindrical MPZs and controlled implants after four weeks. (a-c) 3D reconstructed micro-CT images of new bone tissue formed around the implanted KNN (a), MPZs (b) and HA (c) cylinders, respectively. The pink color shows the regenerated new bone, whereas the yellow color shows the implants. (a1-c1) are the microscopies of hematoxylin-eosin staining of the bone/implant interface of KNN (a1), MPZs (b1) and HA (c1) cylinders, respectively. (a2, c2) are backscattered-electron SEM images of the bone/implant interface of KNN (a2), MPZs (b2) and HA (c2) cylinders. All results indicate that that the MPZs sample induced and promoted bone regeneration most efficiently among all three groups.

In vivo osteogenic performance

Because the microscale piezoelectric structures (MPZs) mimic bone in terms of piezoelectricity, they could promote cell adhesion and proliferation and induce osteogenic differentiation in the absence of additional chemical inducers. We further conducted an animal implantation experiment to assess the *in vivo* bone regeneration in proximity to the polarized MPZs and two controls (KNN and HA). To compare the bone regeneration on the MPZ group with the control groups, the cylindrical samples (3 mm in diameter) of the MPZ group and the two control group were fabricated as rods using the same sintering process and laser-irradiation parameters as applied to the ceramic plates. After poling, the samples were implanted into the New Zealand rabbit femoral condyles. Bone growth was evaluated 4 weeks after implantation by harvesting the femoral bones with the implants. The samples were analyzed with micro-CT. 3D reconstructions of the micro-CT images revealed that the MPZs could significantly induce bone regeneration and achieved greater bone repair than the other groups (**Figure 6a-c**, where the newly grown bones are shown in green and the implant samples are shown in yellow). The quantitative analysis of the micro-CT images indicates that new bone tissue formed on the MPZ group is more than that on the other control groups (**Figure S6**).

In the *in vivo* environment, because of the slight movements and vibrations of the body, a dynamic electrical cue would be induced on the surface of the MPZs samples, mimicking the electrical cue exerted by the piezoelectric collagen fiber pattern in the native bone tissue [44]. The 3D reconstruction of the implants and bone interface confirmed that this dynamic electrical cue from the MPZs implant could more efficiently promote the bone regeneration process than the unmodified KNN (Figure 6a-c). In addition, both histological (Figure 6a1-c1) and backscattered-SEM observation (Figure 6a2-c2) of the implants suggest that more newly formed bone covered the polarized MPZs surface than the

polarized KNN and HA surface. The newly formed bone tissue with osteocytes in lacunae could be observed on the MPZ groups. Furthermore, the newly formed bone was firmly attached to the MPZ implants surface as shown in the backscattered-SEM image. However, the woven bone of KNN and HA groups were lined by osteoblasts, suggesting that bone formation on the interface was still in progress. All the results proved the enhanced bone regeneration around the MPZs implant surface.

The advanced bone regeneration ability of the MPZs could be attributed to the spatially specific electrical cue generated by the MPZs. Electric stimulation has been widely used to modulate stem cell differentiation and bone regeneration in the previous studies [45, 46]. However, no previous study was focused on simulating the microzoned piezoelectric property of the native bone to provide effective electric stimulation to the stem cells for bone regeneration. The MPZs could simulate the spatially specific piezoelectricity of the native bone. When being implanted into the bone, the MPZs would act as a dynamic electrical cue source like the extracellular matrix of natural bone. It is possible that the bone-like spatially specific electrical cues can favor the recruitment of BMSCs from the surrounding healthy tissue to the bone defect site. Then the BMSCs are induced to differentiate into osteoblasts for bone regeneration. As the piezoelectricity represents the electrical microenvironment of natural bone, the use of microscale piezoelectric materials to mimic a bone-like electrical microenvironment will have substantial implications for future design of bone regenerative materials [47].

Summary

This study described the construction of periodically organized MPZs to mimic the piezoelectricity distribution in the natural bone to induce osteogenic differentiation and bone regeneration. A selective laser-irradiation process was introduced to create microzones with piezoelectricity differences and construct electroactive MPZs on the KNN surface to mimic the spatially specific distribution of functionalized piezoelectric structures in bone. The hierarchical MPZs surface could induce osteogenic differentiation *in vitro* and bone regeneration *in vivo*. The use of microscale piezoelectric materials to mimic *in vivo* electrical microenvironment will shed light on the manipulation of stem cell behavior and tissue regeneration by controlling piezolectric cues.

Acknowledgements

This study was supported by the National High Technology Research and Development Program of China (863 Program) (2015AA033502), the National Natural Science Foundation of China (51372087, 51232002, 51541201, 51673168), Science and Technology Planning Project of Guangdong Province, China (2014A010105048), the Natural Science Foundation of Guangdong Province (2015A030313493, 2016A030308014) and State Key Laboratory for Mechanical Behavior of Materials, China (Grant No. 20141607). YZ and CBM would also like to thank the financial support from National Institutes of Health (CA200504, CA195607, and EB021339), Oklahoma Center for Adult Stem Cell Research (434003), and Oklahoma Center for the Advancement of Science and Technology (HR14-160).

Author contributions

P.Y., C.Y.N, and C.B.M. conceived the ideas and designed the concept. P.Y. and C.Y.N conducted the material design experiments and analysed the data. P.Y., X.L.W., G.X.T, X.Y. and Y.Zhu. designed and worked on the cellular assay. P.Y., Y.Zhang, Z.F.L, S.X.L., H.Q.Y., Y.Zhu and K.L. designed and worked on the animal experiment and relative analysis. P.Y., C.Y.N, and C.B.M. interpreted the data and wrote the manuscript.

Supplementary Material

Supplementary figures.
http://www.thno.org/v07p3387s1.pdf

Competing Interests

The authors have declared that no competing interest exists.

References

1. Murphy WL, McDevitt TC, Engler AJ. Materials as stem cell regulators. Nat Mater. 2014; 13: 547-57.
2. Monge C, Saha N, Boudou T, Pozos-Vasquez C, Dulong V, Glinel K, et al. Rigidity-Patterned Polyelectrolyte Films to Control Myoblast Cell Adhesion and Spatial Organization. Adv Funct Mater. 2013; 23: 3432-42.
3. Lane SW, Williams DA, Watt FM. Modulating the stem cell niche for tissue regeneration. Nat Biotechnol. 2014; 32: 795-803.
4. Danoux C, Sun LY, Kocer G, Birgani ZT, Barata D, Barralet J, et al. Development of Highly Functional Biomaterials by Decoupling and Recombining Material Properties. Adv Mater. 2016; 28: 1803-8.
5. Cao BR, Yang MY, Mao CB. Phage as a genetically modifiable supramacromolecule in chemistry. Acc Chem Res. 2016; 49: 1111-20.
6. Sunderland KS, Yang MY, Mao CB. Phage-enabled nanomedicine: from probes to therapeutics in precision medicine. Angew Chem Int Edit. 2017: 1964-92.
7. Engler AJ, Sen S, Sweeney HL, Discher DE. Matrix elasticity directs stem cell lineage specification. Cell. 2006; 126: 677-89.
8. Yang HB, Nguyen KT, Leong DT, Tan NS, Tay CY. Soft Material Approach to Induce Oxidative Stress in Mesenchymal Stem Cells for Functional Tissue Repair. Acs Appl Mater Inter. 2016; 8: 26591-9.
9. Tay CY, Yu HY, Pal M, Leong WS, Tan NS, Ng KW, et al. Micropatterned matrix directs differentiation of human mesenchymal stem cells towards myocardial lineage. Exp Cell Res. 2010; 316: 1159-68.
10. Tay CY, Koh CG, Tan NS, Leong DT, Tan LP. Mechanoregulation of stem cell fate via micro-/nano-scale manipulation for regenerative medicine. Nanomedicine-Uk. 2013; 8: 623-38.
11. Yu HY, Tay CY, Pal M, Leong WS, Li HQ, Li H, et al. A Bio-inspired Platform to Modulate Myogenic Differentiation of Human Mesenchymal Stem Cells Through Focal Adhesion Regulation. Adv Healthc Mater. 2013; 2: 442-9.

12. Wang JL, Wang L, Yang MY, Zhu Y, Tomsia A, Mao CB. Untangling the effects of peptide sequences and nanotopographies in a biomimetic niche for directed differentiation of iPSCs by assemblies of genetically engineered viral nanofibers. Nano Lett. 2014: 6850-6.
13. Wieland DCF, Krywka C, Mick E, Willumeit-Romer R, Bader R, Kluess D. Investigation of the inverse piezoelectric effect of trabecular bone on a micrometer length scale using synchrotron radiation. Acta Biomater. 2015; 25: 339-46.
14. Marino A, Becker RO. Piezoelectric effect and growth control in bone. Nature. 1970; 228: 473-4.
15. Shamos MH, Lavine LS, Shamos MI. Piezoelectric effect in bone. Nature. 1963; 197: 81.
16. Feng JQ, Yuan HP, Zhang XD. Promotion of osteogenesis by a piezoelectric biological ceramic. Biomaterials. 1997; 18: 1531-4.
17. Minary-Jolandan M, Yu MF. Uncovering Nanoscale Electromechanical Heterogeneity in the Subfibrillar Structure of Collagen Fibrils Responsible for the Piezoelectricity of Bone. Acs Nano. 2009; 3: 1859-63.
18. Palmer LC, Newcomb CJ, Kaltz SR, Spoerke ED, Stupp SI. Biomimetic Systems for Hydroxyapatite Mineralization Inspired By Bone and Enamel. Chem Rev. 2008; 108: 4754-83.
19. Nair AK, Gautieri A, Chang SW, Buehler MJ. Molecular mechanics of mineralized collagen fibrils in bone. Nat Commun. 2013; 4.
20. Brown CP, Boyd JL, Palmer AJ, Phillips M, Couture CA, Rivard M, et al. Modulation of Mechanical Interactions by Local Piezoelectric Effects. Adv Funct Mater. 2016; 26: 7662-7.
21. Song B, Gu Y, Pu J, Reid B, Zhao ZQ, Zhao M. Application of direct current electric fields to cells and tissues in vitro and modulation of wound electric field in vivo. Nat Protoc. 2007; 2: 1479-89.
22. Ning CY, Zhou L, Tan GX. Fourth-generation biomedical materials. Mater Today. 2016; 19: 2-3.
23. Cohen DJ, Nelson WJ, Maharbiz MM. Galvanotactic control of collective cell migration in epithelial monolayers. Nat Mater. 2014; 13: 409-17.
24. Ning CY, Yu P, Zhu Y, Yao MY, Zhu XJ, Wang XL, et al. Built-in microscale electrostatic fields induced by anatase-rutile-phase transition in selective areas promote osteogenesis. Npg Asia Mater. 2016; 8.
25. Ahn CH, Rabe KM, Triscone JM. Ferroelectricity at the nanoscale: Local polarization in oxide thin films and heterostructures. Science. 2004; 303: 488-91.
26. Pramanick A, Jorgensen MRV, Diallo SO, Christianson AD, Fernandez-Baca JA, Hoffmann C, et al. Nanoscale Atomic Displacements Ordering for Enhanced Piezoelectric Properties in Lead-Free ABO(3) Ferroelectrics. Adv Mater. 2015; 27: 4330-5.
27. Yu P, Zhu XJ, Wang XL, Wang SY, Li WP, Tan GX, et al. Periodic Nanoneedle and Buffer Zones Constructed on a Titanium Surface Promote Osteogenic Differentiation and Bone Calcification In Vivo. Adv Healthcare Mater. 2016; 5: 364-72.
28. Lu JP, Lim X, Zheng MR, Mhaisalkar SG, Sow CH. Direct Laser Pruning of CdSxSe1-x Nanobelts en Route to a Multicolored Pattern with Controlled Functionalities. Acs Nano. 2012; 6: 8298-307.
29. Lin DM, Kwok KW, Chan HLW. Effect of Alkali Elements Content on the Structure and Electrical Properties of (K0.48Na0.48Li0.04)(Nb0.90Ta0.04Sb0.06)O-3 Lead-Free Piezoelectric Ceramics. J Am Ceram Soc. 2009; 92: 2765-7.
30. Bortolani F, del Campo A, Fernandez JF, Clemens F, Rubio-Marcos F. High Strain in (K,Na)NbO3-Based Lead-Free Piezoelectric Fibers. Chem Mater. 2014; 26: 3838-48.
31. Wang K, Yao FZ, Jo W, Gobeljic D, Shvartsman VV, Lupascu DC, et al. Temperature-Insensitive (K,Na)NbO3-Based Lead-Free Piezoactuator Ceramics. Adv Funct Mater. 2013; 23: 4079-86.
32. Fu DW, Cai HL, Liu YM, Ye Q, Zhang W, Zhang Y, et al. Diisopropylammonium Bromide Is a High-Temperature Molecular Ferroelectric Crystal. Science. 2013; 339: 425-8.
33. Li LL, Lu L, Wang ZG, Li YX, Yao YG, Zhang DW, et al. Anatomy of vertical heteroepitaxial interfaces reveals the memristive mechanism in Nb2O5-NaNbO3 thin films. Sci Rep. 2015; 5.
34. Pina S, Oliveira JM, Reis RL. Natural-Based Nanocomposites for Bone Tissue Engineering and Regenerative Medicine: A Review. Adv Mater. 2015; 27: 1143-69.
35. Levin M. Large-scale biophysics: ion flows and regeneration. Trends Cell Biol. 2007; 17: 261-70.
36. Zhou Y, Wong CO, Cho KJ, van der Hoeven D, Liang H, Thakur DP, et al. Membrane potential modulates plasma membrane phospholipid dynamics and K-Ras signaling. Science. 2015; 349: 873-6.
37. Wang CC, Lu JN, Young TH. The alteration of cell membrane charge after cultured on polymer membranes. Biomaterials. 2007; 28: 625-31.
38. Hamdan M, Blanco L, Khraisat A, Tresguerres IF. Influence of titanium surface charge on fibroblast adhesion. Clin Implant Dent R. 2006; 8: 32-8.
39. Schneider GB, English A, Abraham M, Zaharias R, Stanford C, Keller J. The effect of hydrogel charge density on cell attachment. Biomaterials. 2004; 25: 3023-8.
40. Allen GM, Mogilner A, Theriot JA. Electrophoresis of Cellular Membrane Components Creates the Directional Cue Guiding Keratocyte Galvanotaxis. Curr Biol. 2013; 23: 560-8.
41. Yao X, Peng R, Ding JD. Cell-Material Interactions Revealed Via Material Techniques of Surface Patterning. Adv Mater. 2013; 25: 5257-86.
42. Zheng CP, Wang JS, Liu YN, Yu QQ, Liu Y, Deng N, et al. Functional Selenium Nanoparticles Enhanced Stem Cell Osteoblastic Differentiation through BMP Signaling Pathways. Adv Funct Mater. 2014; 24: 6872-83.
43. Sanchez-Ferrero A, Mata A, Mateos-Timoneda MA, Rodriguez-Cabello JC, Alonso M, Planell J, et al. Development of tailored and self-mineralizing citric acid-crosslinked hydrogels for in situ bone regeneration. Biomaterials. 2015; 68: 42-53.
44. Ribeiro C, Parssinen J, Sencadas V, Correia V, Miettinen S, Hytonen VP, et al. Dynamic piezoelectric stimulation enhances osteogenic differentiation of human adipose stem cells. J Biomed Mater Res, Part A. 2015; 103: 2172-5.
45. Brighton CT, Wang W, Seldes R, Zhang GH, Pollack SR. Signal transduction in electrically stimulated bone cells. J Bone Joint Surg Am. 2001; 83A: 1514-23.
46. Goldenberg DM, Hansen HJ. Electric enhancement of bone healing. Science. 1972; 175: 1118-20.
47. Rajabi AH, Jaffe M, Arinzeh TL. Piezoelectric materials for tissue regeneration: A review. Acta Biomater. 2015; 24: 12-23.